JOURNAL OF SOLID STATE CHEMISTRY 100, 292–300 (1992)

Structure and Magnetic Properties of $Pr_{1-x}Sr_xMnO_3$ Perovskites

K. KNÍŽEK, Z. JIRÁK,* E. POLLERT, F. ZOUNOVÁ

Institute of Physics, 162 00 Prague 6, Czechoslovakia

AND S. VRATISLAV

Faculty of Nuclear Physics and Physical Engineering, 180 00 Prague 8, Czechoslovakia

Received December 20, 1991; in revised form April 20, 1992; accepted March 25, 1992

A comprehensive account of structural features in mixed Mn^{3+}, Mn^{4+} perovskites, $Pr_{1-x}A_xMnO_3$ (A = Ca, Sr, Ba) is given. The newly investigated Sr system was studied at various temperatures by X-ray and neutron diffraction, magnetic, and conductivity measurements. A low-temperature transition from the activated type to the degenerate type of conductivity was observed in the Sr system for x = 0.3–0.4. It occurs 20–60 K below the ferromagnetic Curie point. © 1992 Academic Press, Inc.

Introduction

Manganese oxide perovskites with coexisting Mn^{3+}, Mn^{4+} ions have received much attention both in fundamental and applied solid state chemistry. The most studied systems are the lanthanum-based manganites $La^{3+}_{1-x}A^{2+}_x(Mn^{3+}_{1-x}Mn^{4+}_x)O_3$ ($A = Ca^{2+}, Sr^{2+}, Ba^{2+}$, or Pb^{2+}), which for $0.2 \leq x \leq 0.5$ are ferromagnets with metallic conductivity and Curie temperature as high as 370 K (*1*). Stability of these oxides even above 1000°C, appreciable electronic conductivity, resistance against reactivity with yttria-stabilized zirconia electrolytes, and electrocatalytic properties for the reduction of oxygen make them suitable cathodic materials for the high-temperature solid oxide fuel cells (see, e.g., (*2, 3*)). Similar properties and potential applications are expected for related rare-earth manganites $Pr_{1-x}A_xMnO_3$ or $Nd_{1-x}A_xMnO_3$. The present structural study deals namely with the $Pr_{1-x}Sr_xMnO_3$ series and has been carried out as a complement of our previous investigation of systems $Pr_{1-x}Ca_xMnO_3$ ($0 \leq x \leq 1$) (*4, 5*) and $Pr_{1-x}Ba_xMnO_3$ ($0 \leq x \leq 0.4$) (*6*).

There are two characteristic distortions which influence the perovskite structure of mixed manganites. One consists of a cooperative tilting of MnO_6 octahedra and is established below ~1000 K. This kind of distortion is a consequence of the ionic radii mismatch and is common in perovskites with small central cations (Goldschmidt's tolerance factor <1). The other kind of structural distortion is connected with the Jahn–Teller effect of Mn^{3+} ions leading to the distortion of $Mn^{3+}O_6$ octahedra and their cooperative ordering below certain critical temperature.

The $Pr_{1-x}Ca_xMnO_3$ system shows in the whole range of concentrations ($0 \leq x \leq 1$) a

* To whom correspondence should be addressed.

0022-4596/92 $5.00

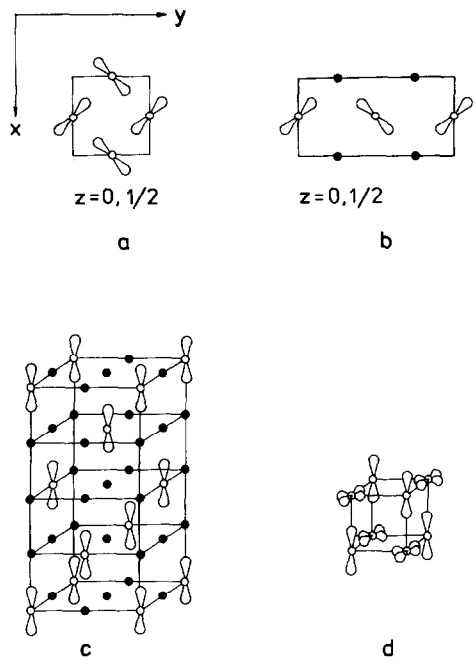

FIG. 1. The valence and d_γ orbital ordering in $Pr_{1-x}Ca_xMnO_3$ (5) for (a) $x = 0$, (b) $x = 0.5$, and (c) $x = 0.75$ (Mn^{4+} sites shown by full dots, Mn^{3+} by lobes); (d) expected arrangement in the dilute Mn^{3+} system $Pr_{0.65}Ba_{0.35}MnO_3$ (6).

double tilting of MnO_6 octahedra (so-called buckling) which leads to an orthorhombic phase of the *Pbnm* symmetry and quadruple cell $\sqrt{2}a_p \times \sqrt{2}a_p \times 2a_p$ compared with the ideal cubic perovskite. The lattice deformation is relatively small and is characterized by a relationship $a \lesssim c/\sqrt{2} \lesssim b$ (the so-called O-type structure).

At lower temperatures where the cooperative Jahn–Teller ordering takes place, the $Pr_{1-x}Ca_xMnO_3$ system can be divided into four compositional regions with different ordering of Mn^{3+} ions and their d_γ orbitals ($0 \lesssim x \lesssim 0.3$, $0.3 \lesssim x \lesssim 0.75$, $0.75 \lesssim x \lesssim 0.9$, and $0.9 \lesssim x \lesssim 1$) (5). $PrMn^{3+}O_3$ ($x = 0$) is a structural prototype in the first region, where orbital ordering of the type shown in Fig. 1a appears. This orbital ordering does not change the *Pbnm* symmetry but modifies and enhances the lattice deformation in such a way that $c/\sqrt{2} \lesssim a \lesssim b$ (the O′-type structure). The critical temperature of the Jahn–Teller transition being ~820 K for pure $PrMnO_3$ is quickly lowered when the concentration of Mn^{3+} ions is decreased. In the next region $0.3 \lesssim x \lesssim 0.75$ the samples are pseudocubic at room temperature and below ~250 K they undergo Jahn–Teller transition to a pseudotetragonal compressed phase T. The structural prototype of this phase is $x = 0.5$, where ordering of the Mn^{3+}/Mn^{4+} (1 : 1) type shown in Fig. 1b exists. In the range of $0.75 \lesssim x \lesssim 0.9$ an ordering of the Mn^{3+}/Mn^{4+} (1 : 3) type, resulting in a pseudotetragonal elongated phase T′, takes place below the critical temperature of ~200 K (see prototype with $x = 0.75$ shown in Fig. 1c). Finally, a pseudocubic structure of the O-type mentioned above exists for $0.9 \lesssim x \lesssim 1$ and the structural prototype is $CaMn^{4+}O_3$ ($x = 1$).

A different situation occurs in the $Pr_{1-x}Ba_xMnO_3$ series (6). Due to the large size of Ba^{2+} ions, the perovskite structure exists only in a limited region up to $x \sim 0.4$, in which two closely related orthorhombic phases can be distinguished. In the range $0 \lesssim x \lesssim 0.2$, the structure is of the O′-type as in the first region of the $Pr_{1-x}Ca_xMnO_3$ series. The orthorhombic deformation decreases more quickly, however, so for $x = 0.2$ there is no observable difference from the cubic metrics. Lattice deformation is established again for $0.2 < x \lesssim 0.4$ where the second orthorhombic phase exists. This phase is of the *Ibmm* symmetry and exhibits a single tilting of MnO_6 octahedra along the orthorhombic *b*-axis only. The samples close to the perovskite phase boundary $x \sim 0.4$ undergo below ~300 K a transition from the *Ibmm* structure to a tetragonal elongated phase of the *I4/mcm* symmetry which is characterized by a different tilting. In addition, large local distortion of MnO_6 octahedra were detected at low temperatures. These distortions are possibly long-range correlated, as shown in Fig. 1d.

The knowledge of structural details helps to understand the magnetism in the mixed manganese oxides. In $Pr_{1-x}Ca_xMnO_3$, the type of the Mn^{3+}, Mn^{4+} valence distribution realized and presence of extra holes or electrons substantially influence magnetic interactions between magnetic spins. As a consequence, diverse magnetic structures are observed at low temperatures (*5*). In most cases their occurrence can be explained by an interplay of two possible interactions between nearest cations, namely, the superexchange (*7*) and the double exchange (*8*).

Magnetic behavior of $Pr_{1-x}Ba_xMnO_3$ is much simpler. The magnetic arrangement is changed with increasing x from the layer-type antiferromagnetism for $x = 0$ to a canted ferromagnetism as in the first, Mn^{3+}-rich region, of the calcium series. For $x > 0.2$ the samples become pure ferromagnets and exhibit below the Curie temperature a transition from the activated type to a degenerate type of conductivity. No such transition has been detected for $Pr_{1-x}Ca_xMnO_3$ in its rather narrow ferromagnetic region $0.2 \leq x \leq 0.3$.

In the presently investigated system $Pr_{1-x}Sr_xMnO_3$, the size of the doping cation is intermediate between Ca^{2+} and Ba^{2+} ions. The Goldschmidt's tolerance factor is 0.92 and 1.04 for $PrMnO_3$ and $SrMnO_3$, respectively (ionic radii taken from Ref. (*9*) for coordination number of Pr and Sr 12). This suggests that the perovskite structure is unstable for the latter compound and, in fact, $SrMnO_3$, like $BaMnO_3$, forms hexagonal phases under ambient conditions. Following the conception of the tolerance factor, the perovskite phase up to ~0.6 may be anticipated.

Experimental

Ceramic synthesis of $Pr_{1-x}Sr_xMnO_3$ has been done up to maximum strontium content $x = 0.6$ starting from appropriate amounts of Pr_6O_{11}, $SrCO_3$, and $MnCO_3$. The mixtures were calcined at 850°C, pressed into pellets, and repeatedly sintered in air (for $x = 0.5$ and 0.6 in oxygen) with intermediate grinding, finally at 1340–1260°C for 48–120 hr and furnace cooled. The sample labeled 0.4b (see below) was quenched into air. The phase analysis and the determination of the lattice parameters at room temperature and, for some samples, at low and high temperatures were carried out on a diffractometer DRON-3 using Cu$K\alpha$ radiation filtered by Ni-filter, λ(Cu$K\alpha$) = 1.54178 Å. The oxygen content was determined by the wet chemical analysis based on the reduction of $Mn^{3+,4+}$ by Fe^{2+}. Complete determination of the crystal structure for $x = 0.1$, 0.3, and 0.5 samples was achieved by powder neutron diffraction (λ = 1.364 Å) on the diffractometer KSN-2 of the reactor in Řež near Prague. The diffraction patterns recorded were refined using the standard Rietveld profile method. In addition, neutron diffraction patterns at selected low temperatures (down to 5 K) were recorded in order to determine the magnetic arrangements.

The measurement of the dependence of magnetic susceptibility on temperature and magnetic field was performed on the Foner-type magnetometer in an applied field up to 2.5 T. Temperature dependence (range 12–300 K) of the conductivity was investigated on samples of dimensions 1.5 × 1 × 5 mm^3 using the standard four-probe technique.

Results

1. X-ray Measurement

The single-phase samples were found in the range of $x \leq 0.5$, while for $x = 0.6$ a presence of the $SrMnO_3$ 4-layer hexagonal phase was observed. From the intensity of the $SrMnO_3$ reflections we estimate the limit of Sr substitution to be slightly below 0.6.

Lattice constants, quantity D characterizing the orthorhombic deformation, and Mn^{3+}, Mn^{4+} valence distribution based on

TABLE I

LATTICE PARAMETERS, ORTHORHOMBIC DEFORMATION, THE Mn^{3+}/Mn^{4+} VALENCE DISTRIBUTION, AND THE OXYGEN STOICHIOMETRY

x	a	b	c	$c/\sqrt{2}$[Å]	D[%]	Composition
0	5.454	5.809	7.587	5.365	3.19	$PrMnO_3$[a]
0.1	5.472(1)	5.632(1)	7.657(2)	5.414(2)	1.52	$Pr_{0.9}Sr_{0.1}Mn^{3+}_{0.856}Mn^{4+}_{0.144}O_{3.022}$
0.2	5.479(3)	5.485(3)	7.732(3)	5.468(3)	0.12	$Pr_{0.8}Sr_{0.2}Mn^{3+}_{0.722}Mn^{4+}_{0.228}O_{3.014}$
0.3	5.486(3)	5.467(3)	7.713(5)	5.454(3)	0.21	$Pr_{0.7}Sr_{0.3}Mn^{3+}_{0.689}Mn^{4+}_{0.311}O_{3.006}$
0.4b	5.486(3)	5.442(3)	7.674(5)	5.426(4)	0.42	$Pr_{0.6}Sr_{0.4}Mn^{3+}_{0.633}Mn^{4+}_{0.367}O_{2.984}$
0.4	5.449(2)	5.430(2)	7.674(3)	5.426(2)	0.17	$Pr_{0.6}Sr_{0.4}Mn^{3+}_{0.561}Mn^{4+}_{0.439}O_{3.019}$
0.5	5.443(3)	5.423(2)	7.644(3)	5.405(2)	0.24	$Pr_{0.5}Sr_{0.5}Mn^{3+}_{0.450}Mn^{4+}_{0.550}O_{3.025}$

Note. $D = \frac{1}{3}\sum_{i=1}^{3} |(a_i - \bar{a})/\bar{a}| \times 100$, $a_1 = a$, $a_2 = b$, $a_3 = c/\sqrt{2}$, $\bar{a} = (abc/\sqrt{2})^{1/3}$

[a] See Ref. (*4*).

the oxygen content (assuming trivalent praseodymium ions only) are given in Table I. With the exception of 0.4b, the samples show a slight excess of oxygen which increases the Mn^{4+} content over the nominal one. All the samples prepared exhibit perovskite related structure of the *Pbnm* symmetry. The orthorhombic deformation decreases rapidly from $D = 3.19\%$ for $x = 0$ to $D = 0.12\%$ for $x = 0.2$, and then increases slightly to $D \cong 0.20\%$ for $x = 0.3$–0.5 (see Table I and Fig. 2). Sample $x = 0.4$b shows a larger deformation which might be a specifier manifestation of the oxygen deficiency. The sample is included because of its Curie temperature and specific conductivity are the greatest of all samples.

The dependence of lattice parameters on temperature was studied for sample with $x = 0.1$ at high temperatures and for samples with $x = 0.3$–0.5 at low temperatures. The results for $x = 0.1$, illustrated in Fig. 3, show a transition from the O′-type structure ($c/\sqrt{2} < a < b$) to the O-type ($c/\sqrt{2} \cong a < b$) at 350°C. At low temperatures there are no marked changes except for the sample with $x = 0.5$, which exhibits below 160 K a sudden change of lattice parameters—shortening c, elongating a, b (see Fig. 4). This is a consequence of the Mn^{3+}/Mn^{4+} (1 : 1) ordering shown above in Fig. 1b. For $x = 0.1$, 0.3, and 0.5, the lattice parameters at 5 K were obtained by neutron diffraction and,

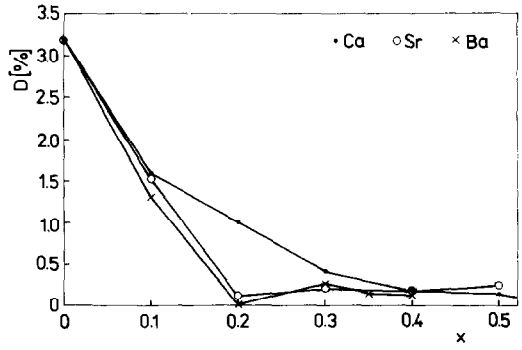

FIG. 2. The orthorhombic deformation in $Pr_{1-x}A_xMnO_3$ (A = Ca, Sr, Ba).

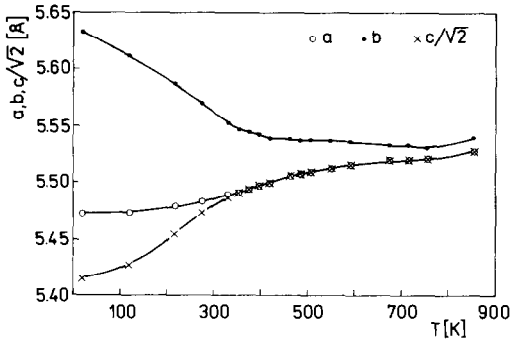

FIG. 3. The temperature dependence of lattice parameters for $Pr_{0.9}Sr_{0.1}MnO_3$.

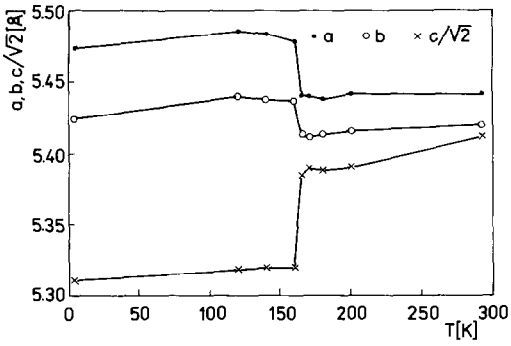

FIG. 4. The low-temperature transition in $Pr_{0.5}Sr_{0.5}MnO_3$.

together with the values of orthorhombic deformation, are given in Table II.

2. Neutron Measurement for $x = 0.1$, 0.3, and 0.5

Positional parameters of all atoms, the Debye–Waller coefficient of an overall temperature factor, Mn–O distances, Mn–O–Mn angles and magnetic moments observed at 5 K are given in Table III. For $x = 0.1$ the MnO_6 octahedra are tetragonally elongated with the long Mn–O bond in the (001) plane. The MnO_6 octahedra appears to be regular within the estimated standard deviations for the other samples $x = 0.3$ and 0.5.

The positional parameters for $x = 0.5$ at the helium temperature were obtained assuming the *Pbnm* symmetry and should be, therefore, considered as approximate. As discussed in Ref. (*5*) the structure is in fact monoclinic with a doubled elementary cell compared with the *Pbnm* phase. A single-crystal diffractometry would be needed for a more complete structure determination.

TABLE II

LATTICE PARAMETERS AND DEFORMATION AT 5 K

x	a	b	c	$c/\sqrt{2}$[Å]	D[%]
0.1	5.460(1)	5.618(1)	7.626(2)	5.391(2)	1.55
0.3	5.474(3)	5.445(2)	7.686(4)	5.435(3)	0.28
0.5	5.472(4)	5.424(4)	7.511(8)	5.311(6)	1.13

The orthorhombic deformation of samples $x = 0.3$ and $x = 0.5$ is small compared with the resolution of the neutron powder diffraction. Nevertheless, the Rietveld profile analysis succeeded to refine lattice parameters in agreement with the line splitting observed by the X-ray diffraction. More importantly, the a and b parameters were found to be reversed ($a > b$), which is an unexpected result in orthoperovskites. The effect is more pronounced at lower temperatures (see Tables I and II).

The magnetic structure for $x = 0.1$ is related to that of pure $PrMnO_3$ (*10*) which is so-called *A*-type or layer antiferromagnet with ferromagnetically arranged Mn moments within the (001) layers and antiferromagnetic coupling between the layers. The moments are oriented along the y-axis. For $x = 0.1$, in contrary, there is a canting between the layers leading to a net magnetic moment. The observed ferromagnetic and antiferromagnetic components are practically equal (canting angle 90°), μ_F lies in the z-axis, and μ_{AF} lies in the y-axis. This implies that the resulting magnetic moments are along the directions [011] and $[0\bar{1}1]$ in layers $z = 0$ and 0.5, respectively. The canting persists up to the paramagnetic transition at 85 K.

The sample $x = 0.3$ is a pure ferromagnet with magnetic moments along the x-axis, which turns now to be longest of the two basal axes. Sample $x = 0.5$ exhibits ferromagnetic ordering only in a limited range below $T_c = 200$ K. Then at the above-mentioned phase transition at 160 K a purely antiferromagnetic structure of the so-called CE type (*7, 11*), shown also in the inset of Fig. 5, arises. Observed magnetic moments for the Mn^{3+} and Mn^{4+} sites are practically equal and are oriented along the x-axis. The magnetic transitions for $x = 0.5$ are illus-

TABLE III

NEUTRON DIFFRACTION DATA FOR $Pr_{1-x}Sr_xMnO_3$ (SPACE GROUP *Pbnm*)

		T = 300 K			T = 5 K		
	x	0.1	0.3	0.5	0.1	0.3	0.5
Mn	x	0.500	0.500	0.500	0.500	0.500	0.500
	y	0	0	0	0	0	0
	z	0	0	0	0	0	0
Pr,Sr	x	−0.018(3)	0.005(5)	−0.009(4)	−0.006(3)	−0.012(5)	−0.018(24)
	y	0.049(3)	0.025(2)	0.027(2)	0.061(2)	0.027(2)	0.068(5)
	z	0.250	0.250	0.250	0.250	0.250	0.250
O_I	x	0.075(3)	0.068(3)	0.062(3)	0.076(2)	0.061(5)	0.058(7)
	y	0.486(2)	0.495(3)	0.493(3)	0.483(1)	0.494(3)	0.544(9)
	z	0.250	0.250	0.250	0.250	0.250	0.250
O_{II}	x	−0.284(2)	−0.276(4)	−0.269(3)	−0.280(1)	−0.272(3)	−0.273(6)
	y	0.297(1)	0.276(4)	0.269(3)	0.297(1)	0.275(3)	0.271(6)
	z	0.039(1)	0.034(1)	0.028(2)	0.040(1)	0.032(2)	0.029(4)
B_{overal}		1.1(5)	1.6(3)	1.1(2)	1.0(3)	1.2(3)	
R		5.67	4.99	5.02	4.32	3.52	3.42
$Mn-O_I$		1.96(1)	1.96(1)	1.94(1)	1.95(1)	1.95(1)	1.92(3)
$Mn-O_{II}$		2.07(1)	1.96(2)	1.94(1)	2.08(1)	1.97(2)	1.94(3)
$Mn-O_{II}{}^a$		1.95(1)	1.96(2)	1.94(1)	1.93(1)	1.94(2)	1.96(3)
$Mn-O_I-Mn$		155(1)	158(1)	160(1)	155(1)	160(1)	156(2)
$Mn-O_{II}-Mn$		155(1)	160(1)	165(1)	155(1)	162(1)	164(2)
μ_F					2.09(5)	3.44(6)	0
μ_{AF}					2.11(3)	0	2.20(7)[Mn^{3+}] 2.24(6)[Mn^{4+}]

Note. $O_{II}^a \equiv [x_{O_{II}} + 1/2, \bar{y}_{O_{II}} + 1/2, \bar{z}_{O_{II}}]$.

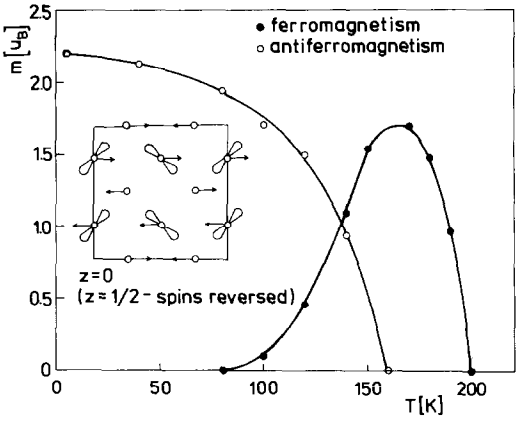

FIG. 5. Temperature course of magnetic ordering in $Pr_{1-x}Sr_xMnO_3$. The inset shows the antiferromagnetic arrangement realized below 160 K.

trated in Fig. 5. This figure is based on a temperature scan of selected magnetic reflections.

3. Magnetic and Conductivity Measurements

Saturated magnetic moments per one manganese ion (in Bohr magnetons), critical temperatures and the type of magnetic arrangement are summarized in Table IV. The ferromagnetic Curie point reaches a maximum above the room temperature for sample 0.4b.

The temperature dependence of resistivity for the system $Pr_{1-x}Sr_xMnO_3$ as well as for selected samples $Pr_{1-x}Ba_xMnO_3$ are plotted in Fig. 6. In both systems, the transition to the metallic state is observed for x =

TABLE IV

MAGNETIC DATA SUMMARY FOR $Pr_{1-x}Sr_xMnO_3$

x	$\langle\mu_{Ne}\rangle$	μ_{mag}	%theory	T_C/T_N	Ordering below T_C/T_N
0.1	2.97(6)	2.35	82	85	Canted
0.2		3.51	97	180	Ferromagnetic
0.3	3.44(6)	3.47	94	259	Ferromagnetic
0.4b		3.35	92	297	Ferromagnetic
0.4		3.35	94	243	Ferromagnetic
0.5	$1.7(1)_{170\ K}$			200	Ferromagnetic
	2.22(6)			160	Antiferromagnetic

Note. $\langle\mu_{Ne}\rangle$-magnetic moment per 1 Mn atom according to neutron diffraction measurement; %theory = μ_{mag}/μ_{spin}, μ_{spin}-the spin-only value for Mn^{3+}, Mn^{4+} ions present.

0.3–0.4. For the strontium $x = 0.5$ sample there is a change of slope in the log ρ/T^{-1} dependence at about 160 K, which is related to the crystallographic transition.

Discussion

Structural and magnetic behavior of the $Pr_{1-x}Sr_xMnO_3$ series display features of the previously investigated systems $Pr_{1-x}Ca_xMnO_3$ and $Pr_{1-x}Ba_xMnO_3$. In the whole single-phase perovskite range ($0 \le x \le 0.5$) the Sr doped samples are of the *Pbnm* symmetry (the $GdFeO_3$ crystal type). At the Mn^{3+}-rich side a more pronounced orthorhombic deformation due to the cooperative Jahn–Teller effect occurs (the O′-type phase). According to powder diffraction data which are available for limited number of the O′-type samples, the MnO_6 octahedra are tetragonally elongated with axial ratio of 1.112 for $PrMn^{3+}O_3$ (*10*), 1.053 for $Pr_{0.9}Ca_{0.1}MnO_3$ (*5*) (actual Mn^{3+} concentration was 91%), and 1.059 for $Pr_{0.8}Sr_{0.1}MnO_3$ (86% Mn^{3+}). For still lower Mn^{3+} concentration the MnO_6 octahedra are practically regular as shown, e.g., by the $Pr_{0.8}Ba_{0.2}MnO_3$ diffraction data (*6*).

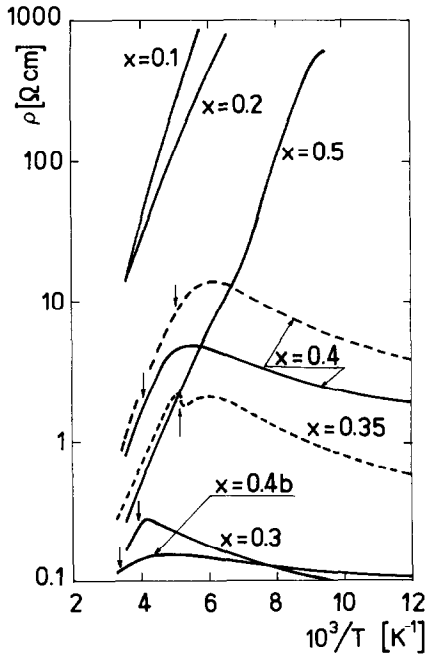

FIG. 6. Resistivity in $Pr_{1-x}Sr_xMnO_3$ and some samples of $Pr_{1-x}Ba_xMnO_3$ (the dotted lines). The arrows mark the ferromagnetic Curie temperatures.

The *Pbnm* structure in $Pr_{1-x}Sr_xMnO_3$ persists for $x < 0.5$ down to low temperatures. The sample $x = 0.5$ undergoes at 160 K a transition to a phase with markedly shortened c-axis ($c/\sqrt{2}$: $(a + b)/2 = 0.975$) in which the buckling of octahedra is combined with the Mn^3/Mn^{4+} (1 : 1) distribution. The orthorhombic deformation is still apparent but otherwise the structure is analogous to the pseudotetragonal T-phase which was observed for the $Pr_{1-x}Ca_xMnO_3$ system (as well as earlier for $La_{1-x}Ca_xMnO_3$ (*7*, *11*)) in broader composition range $0.3 \le x \le 0.7$ and with higher transition temperature ~250 K.

Magnetic ordering in $Pr_{1-x}Sr_xMnO_3$ is similar to the behavior in the Ba series. Observed change with x from the layer-type antiferromagnetism to the pure ferromagnetism is a model situation theoretically treated by de Gennes (*8*). For intermediate canted structures the theory predicts a two-step temperature transition to the paramagnetic state, either through pure antiferromagnetism or pure ferromagnetism, depending on the ratio of the superexchange and the double exchange interactions. In the calcium $x = 0.1$ sample (*5*), the latter case

has been encountered with T_1 (canted → ferromagnetic) = 70 K and T_2 (ferromagnetic → paramagnetic) = 100 K. The coincidence of both temperatures observed in the present study for the strontium $x = 0.1$ sample at 85 K should be considered as accidental.

Different orientations of manganese moments found in the calcium $x = 0.1$ ($m_F \| [110]$, $m_{AF} \| [1\bar{1}0]$) and in the strontium $x = 0.1$ ($m_F \| [001]$, $m_{AF} \| [010]$) are related to different canting angles realized (56° and 90°, respectively). It is in accordance with magnetocristalline anisotropy calculated as a sum of one-ion anisotropies at Mn^{3+} sites (local easy axes along the occupied d_{z^2} orbitals). Necessity of such reorientation may become obvious considering that for limiting angles 0° and 180° (pure ferromagnetism or antiferromagnetism) the magnetic axis should be identical, namely [010]. Apart from the one-ion anisotropies there is of course a lattice term. It might explain the [100] orientation observed in samples $x = 0.3$ and 0.5 which are characterized by a reversal of the a and b parameters.

Canted arrangements vanish apparently at $x = 0.2$ for which in all three series the saturated magnetic moments reach the theoretical spin-only value for the Mn^{3+}, Mn^{4+} ions present. Nevertheless, a small residual antiferromagnetic component of $0.5\mu_B$ (canting angle 18°) was still revealed for the barium $x = 0.2$ compound by the neutron diffraction.

In the ferromagnetic region the Curie temperature increases (the double exchange strengthens due to increasing number of charge carriers) and reaches in $Pr_{1-x}Sr_xMnO_3$ a maximum of 297 K for sample 0.4b. The ferromagnetism develops also in $x = 0.5$, but as soon as the Mn^{3+}/Mn^{4+} (1 : 1) ordering is established at 160 K a characteristic purely antiferromagnetic arrangement is realized.

An interesting property of ferromagnetic manganites is the occurrence of metallic conductivity. As in the Ba series, the $Pr_{1-x}Sr_xMnO_3$ systems exhibits for $x = 0.3$–0.4 a transition from the activated type to the degenerate type of conductivity. It occurs at temperatures 20–60 K below the ferromagnetic Curie points. This is at variance with findings on the lanthanum perovskites, e.g., $La_{1-x}Sr_xMnO_3$ (*1*) or, more evidently, the highly homogeneous sample $La_{0.8}Ca_{0.2}MnO_3$ (*12*) for which the magnetic and conductivity transitions coincided. The distinction of both transitions in the praseodymium systems is best documented for $Pr_{0.65}Ba_{0.35}MnO_3$ in Fig. 6 which shows, apart from the rather broad transition to the metallic conductivity at 160 K, a sharp drop of resistivity exactly at the Curie temperature 190 K. The change of the conductivity character was originally connected with occurrence of large local distortions of MnO_6 octahedra (*6*). The absence of such distortions in the present system $Pr_{1-x}Sr_xMnO_3$ shows, however, that the metallic conductivity has another, for the present unknown, origin.

In conclusion, the mixed oxides $Pr_{1-x}Sr_xMnO_3$ exist in the range $0 \leq x \leq 0.5$ and exhibit the orthoperovskite *Pbnm* structure. The magnetic arrangement is changed from the layer-type antiferromagnetism for $x = 0$ to ferromagnetism for $x > 0.2$. The ferromagnetic samples show a transition to metallic conductivity at low temperatures. For $x = 0.5$, there is a transition below 160 K to a phase with the Mn^{3+}/Mn^{4+} (1 : 1) long-range ordering coupled with a complex antiferromagnetic structure.

References

1. J. H. VAN SANTEN AND G. H. JONKER, *Physica* **16,** 599 (1950).
2. O. YAMAMOTO, Y. TAKEDA, R. KANNO, AND M. NODA, *Solid State Ionics* **22,** 241 (1987).
3. A. HAMMOUCHE, E. SIEBERT, AND A. HAMMON, *Mater. Res. Bull.* **24,** 367 (1989).

4. E. POLLERT, S. KRUPIČKA, AND E. KUZMIČOVÁ, *J. Phys. Chem. Solids* **43,** 1137 (1982).
5. Z. JIRÁK, S. KRUPIČKA, Z. ŠIMŠA, M. DLOUHÁ, AND S. VRATISLAV, *J. Magn. Magn. Mater.* **53,** 153 (1985).
6. Z. JIRÁK, E. POLLERT, A. F. ANDRESEN, J. C. GRENIER, AND P. HAGENMULLER, *Eur. J. Solid State Inorg. Chem.* **27,** 421 (1990).
7. J. B. GOODENOUGH, *Phys. Rev.* **100,** 564 (1955).
8. P. G. DE GENNES, *Phys. Rev.* **118,** 141 (1960).
9. R. D. SHANNON, Acta Crystallogr. Sect. *A* **32,** 751 (1976).
10. S. QUEZEL-AMBRUNAZ, *Bull. Soc. Fr. Mineral Cristallogr.* **91,** 339 (1968).
11. E. O. WOLLAN AND W. C. KOEHLER, *Phys. Rev.* **100,** 545 (1955).
12. J. TANAKA, K. TAKANASHI, K. YUKINO, AND S. HORIUCHI, *Phys. Status Solidi A* **80,** 621 (1983).